ISSN 1674-1056
http://cpb.iphy.ac.cn
http://iopscience.iop.org/cpb
中国物理 B
Chinese Physics
中国物理 Chinese Physics B

Relationship between characteristic lengths and effective Saffman length in colloidal monolayers near a water-oil interface

Na Li(李娜), Wei Zhang(张伟), Wei Chen(陈唯)

Citation: Chin. Phys. B . 2019, 28(6): 064703. **doi:** 10.1088/1674-1056/28/6/064703
Journal homepage: http://cpb.iphy.ac.cn; http://iopscience.iop.org/cpb

What follows is a list of articles you may be interested in

Dramatic change of the self-diffusions of colloidal ellipsoids by hydrodynamic interactions in narrow channels

Han-Hai Li(李瀚海), Zhong-Yu Zheng(郑中玉), Tian Xie(谢天), Yu-Ren Wang(王育人)

Chin. Phys. B . 2019, 28(7): 074701. **doi:** 10.1088/1674-1056/28/7/074701

Characteristics and generation of elastic turbulence in a three-dimensional parallel plate channel using direct numerical simulation

Hong-Na Zhang(张红娜), Feng-Chen Li(李凤臣), Xiao-Bin Li(李小斌), Dong-Yang Li(李东阳), Wei-Hua Cai(蔡伟华), Bo Yu(宇波)

Chin. Phys. B . 2016, 25(9): 094701. **doi:** 10.1088/1674-1056/25/9/094701

Current and efficiency optimization under oscillating forces in entropic barriers

Ferhat Nutku, Ekrem Aydiner

Chin. Phys. B . 2016, 25(9): 090501. **doi:** 10.1088/1674-1056/25/9/090501

Current and efficiency of Brownian particles under oscillating forces in entropic barriers

Ferhat Nutku, Ekrem Aydıner

Chin. Phys. B . 2015, 24(4): 040501. **doi:** 10.1088/1674-1056/24/4/040501

Propulsive matrix of a helical flagellum

Zhang He-Peng, Liu Bin, Bruce Rodenborn, Harry L. Swinney

Chin. Phys. B . 2014, 23(11): 114703. **doi:** 10.1088/1674-1056/23/11/114703

Relationship between characteristic lengths and effective Saffman length in colloidal monolayers near a water–oil interface*

Na Li(李娜)[1,†], Wei Zhang(张伟)[2,†], and Wei Chen(陈唯)[1,‡]

[1] State Key Laboratory of Surface Physics and Department of Physics, Fudan University, Shanghai 200438, China
[2] School of Physical Science and Technology, China University of Mining and Technology, Xuzhou 221116, China

(Received 29 March 2019; revised manuscript received 5 May 2019; published online 29 May 2019)

The hydrodynamic interactions (HIs) in colloidal monolayers are strongly influenced by the boundary conditions and can be directly described in terms of the cross-correlated diffusion of the colloid particles. In this work, we experimentally measured the cross-correlated diffusion in colloidal monolayers near a water–oil interface. The characteristic lengths of the system were obtained by introducing an effective Saffman length. The characteristic lengths of a particle monolayer near a water–oil interface were found to be anisotropic in the longitudinal and transverse directions. From these characteristic lengths, the master curves of cross-correlated diffusion are obtained, which universally describe the HIs near a liquid–liquid interface.

Keywords: colloidal monolayer, cross-correlated diffusion, hydrodynamic interactions, characteristic length

PACS: 47.57.J–, 47.85.Dh, 05.40.Jc, 45.50.–j **DOI:** 10.1088/1674-1056/28/6/064703

1. Introduction

Confined colloidal systems are ubiquitous and important in many real scenarios. Examples of such systems include porous media,[1–3] microfluidic devices,[4–11] proteins in the cytoplasm,[2] and cell membranes.[12–14] The dynamics of a confined colloidal suspension depend on the boundary conditions of the system[15–21] and are more complicated than those of an unbounded free three-dimensional (3D) bulk liquid. Generally, the strength of the hydrodynamic interactions (HIs) between two tracked particles is a function of their separation distance in the liquid.[3,22,23] When a membrane is suspended in a liquid, the HIs in the membrane exhibit a transition from two-dimensional (2D) to 3D in nature with an increasing distance r.[22,24,25] In a quasi-2D system, such as a cell membrane, a liquid–liquid interface, or a liquid film, a characteristic length can be defined to describe the distance at which the crossover from 2D membrane dynamics to 3D bulk dynamics occurs in the liquid.[25–27] When the distance r is much smaller than the characteristic length, both the mass and momentum of the membrane are conserved, as in a 2D membrane,[25,28,29] which results in a decay of the HIs with the distance r as $\ln(1/r)$ due to the contributions of 2D shear stress. When the distance r is greater than the characteristic length, the momentum is transmitted into the surrounding fluid,[13,26] which causes the HIs to decay with the distance r as $1/r$ due to the contributions of the 3D shear stress.

The characteristic lengths of a system depend on the boundary conditions of that system. In the Saffman model,[27,30] the characteristic length of a thin sheet of viscous fluid of viscosity η_s suspended in an unbounded bulk liquid of viscosity η_b is defined as $\lambda_s = \eta_s/\eta_b$, which is called the Saffman length. The characteristic length of a semi-infinite system, such as a viscous film at a water–air interface, is also taken to be equal to the Saffman length $\lambda_s = \eta_s/\eta_b$.[22] However, if the viscous film at the water-air interface is replaced by a colloidal monolayer, the characteristic length of this particle monolayer will depend on both the particle size a and the Saffman length λ_s of the monolayer in the following form: $a(\lambda_s/a)^{3/2}$.[31] When the colloidal monolayer is detached from the interface and placed in bulk water close to the water–air interface, the characteristic lengths in the two orthogonal directions are anisotropic; they are expressed as λ_s and $a(\lambda_s/a)^{2/3}$.[32] However, the characteristic lengths of a particle monolayer near a water–oil interface have not been closely studied until now. We wonder whether characteristic lengths of colloidal monolayers near a water–oil interface can be achieved by the method developed in colloidal monolayers on a water–air interface,[31] and what different features will be exposed between those two systems. When a colloidal monolayer is located near a water–oil interface, momentum diffuses from the colloidal monolayer into the bulk water and bulk oil on either side. In such a scenario, this system can be regarded as similar to a 3D bulk system. However, the HIs in the monolayer will be influenced by the interface, such as that in monolayers near a water–air interface.[32] Thus, it is interesting to consider which kind of HIs behavior can be expected

*Project supported by the National Natural Science Foundation of China (Grant Nos. 11474054, 11774417, and 11604381) and the Natural Science Foundation of Jiangsu Province, China (Grant No. BK20160238).

†These authors contributed equally.

‡Corresponding author. E-mail: phchenwei@fudan.edu.cn

© 2019 Chinese Physical Society and IOP Publishing Ltd

in a colloidal monolayer near a water-oil interface.

In this paper, we report an investigation of the HIs in colloidal monolayers near a water-oil interface that was conducted by experimentally measuring the cross-correlated diffusion of the colloid particles. We find that an effective Saffman length λ_s^* should be introduced in such a system. Using λ_s^*, the characteristic lengths of the colloidal monolayer can be defined, and they are found to be different in the two orthogonal directions. In the longitudinal direction, the characteristic length is equal to λ_s^* itself, while in the transverse direction, the characteristic length exhibits a power-law relationship with λ_s^*. From these characteristic lengths, the friction coefficients of the colloidal monolayers can be estimated, and the results are consistent with those obtained from single-particle measurements. Using the characteristic lengths as scaling factors, universal curves describing the cross-correlated diffusion in a water-oil system are obtained. These universal curves are independent of the separation between the colloidal monolayer and the interface, unlike in the case of a water-air system. Such universal curves can help us to further understand the dynamics of fluids near a soft boundary.

2. Experimental data analysis and discussion

The experimental setup is shown in Fig. 1(a). A stainless steel sample cell with two layered chambers was constructed, similar to that described in Ref. [33]. The chamber for water was 8 mm in width and 0.8 mm in depth. The chamber for oil was 15 mm in width and 1 mm in depth. An aqueous colloidal solution was introduced into the chamber for water such that it filled the chamber. Once the water–air interface was level, decalin was used to fill the oil chamber. The layers of liquid were sandwiched between two coverslips. Finally, the prepared sample was placed upside down and allowed to remain undisturbed for at least two hours. The particle solution was pinned by the edge of the stainless steel hole and remained on top of the layer of decalin. The particles sank under gravity and formed a monolayer close to the water–oil interface. The repulsive interaction of the image charges balanced the action of gravity on the particles, preventing the particles from contacting the water-oil interface. Samples of three kinds of colloid particles were used, namely, silica spheres with radii of $a = 0.6$ μm (S1) and $a = 1.0$ μm (S2), and polystyrene (PS) latex spheres with a radius of $a = 1.0$ μm (S3), as presented in Table 1. Silica spheres with SiO^- groups on their surfaces were purchased from Bangs, and PS spheres with sulfate groups on their surfaces were purchased from Invitrogen. The colloidal samples were cleaned seven times by centrifugation to eliminate any possible surfactant and then suspended in deionized water with a conductivity of 18.2 MΩ · cm. The decalin used was a mixture of cis and trans with a density of 0.896 g/cm^3 and a viscosity of 2.36 cp at a temperature of 28 °C, which was purchased from Sigma–Aldrich. An inverted Olympus IX71 microscope with a 40× objective and a digital camera (Prosilica GE1050, 1024 × 1024 pixels, 14 fps) were used to record the positions of the particles. The spatial resolution was 0.09 μm/pix. Each image sequence consisted of 500 consecutive frames, and each image had dimensions of 176 μm × 176 μm. A typical image obtained by the microscope is shown in Fig. 1(b). Under the frame-collecting rate of 14 fps, particles diffuse a short distance, which is much less than the average separation between the neighbor particles during time intervals between two adjacent frames. The positions of centers of particles were estimated by the geometric mean of positions of pixels. The error of the particle location estimated was half a pixel, *i.e.*, 45 nm in our experiments. Using homemade software (IDL), we obtained the trajectories of the particles with a similar particle tracking algorithm in Ref. [34]. From these particle trajectories, the single-particle diffusion and the correlated diffusion between particles were calculated to study the HIs in the colloidal monolayer.

Table 1. Parameters α, β, γ, and the separation z for three samples.

Samples	a/μm	α	β	γ	$z/upmum$	z/a
S1 silica	0.6	0.74	0.55	2.62	0.73	1.22
S2 silica	1.0	0.78	0.80	0.76	1.46	1.46
S3 PS	1.0	0.86	0.58	1.39	2.29	2.29

First, from the particle trajectories, the particle displacement over a lag time was calculated as $\Delta \boldsymbol{s}_i(\tau) = \boldsymbol{s}_i(t+\tau) - \boldsymbol{s}_i(t)$. The single-particle self-diffusion coefficient $D_s(n)$ was calculated from the mean square displacement using the relation $\langle \Delta s_i^2(\tau) = 4D_s(n)\tau$. As shown in Fig. 1(c), $D_s(n)$ scaled by D_0 is a function of the particle area fraction n, where D_0 is calculated according to the Einstein–Stokes relation: $D_0 = k_B T/6\pi a\eta$. The measurements of this scaled diffusion coefficient $D_s(n)/D_0$ were fit to the following second-order polynomial.[33,35] $D_s(n)/D_0 = \alpha(1 - \beta \cdot n - \gamma \cdot n^2)$. Here, the parameter α is related to the local viscosity experienced by the particles in the dilute limit, and the parameter β is related to the two-body interactions between the particles. When $n \to 0$, the diffusion coefficient $D_s(0)$ can be obtained from the formula $D_s(0)/D_0 = \alpha$; this coefficient is the self-diffusion coefficient of a particle in the monolayer in the dilute limit. From $D_s(0)/D_0$, the separation z from the center of the colloidal monolayer to the water–oil interface was calculated according to Eq. (1):[19,36]

$$\frac{D_s(0)}{D_0} = 1 + \frac{3}{16}\left(\frac{2\eta_w - 3\eta_o}{\eta_w + \eta_o}\right)\left(\frac{a}{z}\right), \tag{1}$$

where η_w is the viscosity of the water and η_o is the viscosity of the decalin. The fitted values of the parameters and the calculated values are shown in Table 1.

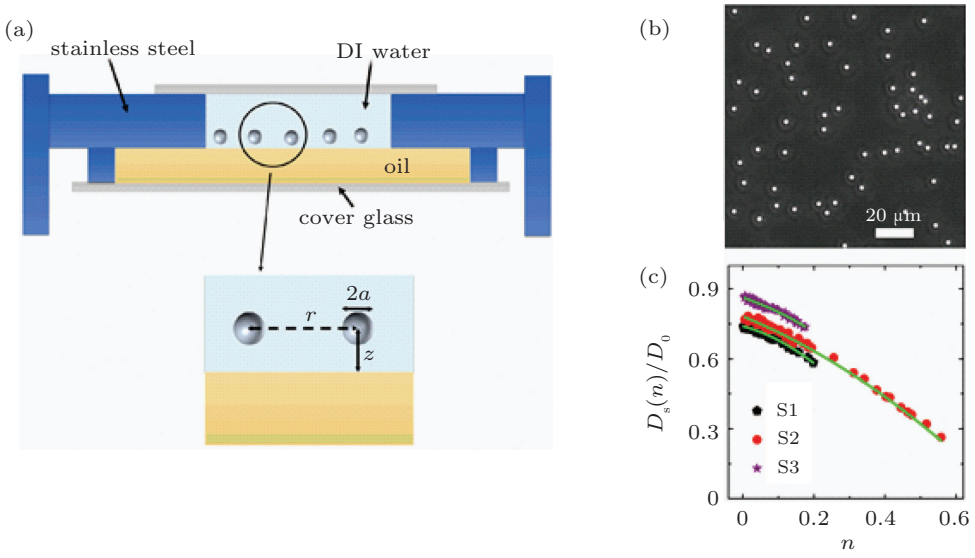


Fig. 1. (a) Schematic illustration of the experimental setup. The distance between particles is denoted by r, the separation from the center of the particle monolayer to the water–oil interface is denoted by z, and the parameter a is the particle radius. (b) Optical microscopic image of silica particles of radius $a = 1.0$ μm suspended near a water–decalin interface at an area fraction of $n = 0.01$. (c) Normalized self-diffusion coefficient $D_s(n)/D_0$ as a function of the area fraction n for each of the three samples: S1 (black pentagon), S2 (red dot), and S3 (purple star). The green curves are fits to the following second-order polynomial $D_s(n)/D_0 = \alpha(1 - \beta \cdot n - \gamma \cdot n^2)$.

From the displacement $\Delta \boldsymbol{s}(\tau)$, the cross-correlated diffusion coefficients $D_{\parallel,\perp}(r)$ were calculated in the directions longitudinal and transverse to the line connecting the centers of two particles (i and j) according to Eq. (2). In Eq. (2), $\parallel$ and $\perp$ represent different coordinates along and perpendicular to the line connecting the centers of particle pair i and j. $\Delta s^i_{\parallel}(t,\tau)$ and $\Delta s^i_{\perp}(t,\tau)$ represent the components of the displacement $\Delta \boldsymbol{s}_i(\tau)$ of particle i at time t during the interval time τ in the longitudinal and transverse directions, respectively. $R^{i,j}(t)$ is the distances between the particles i and j, and the average $\langle \cdots \rangle$ is taken over time t and over all observed particle pairs between which the distances r are equal to $R^{i,j}(t)$.

$$D_{\parallel,\perp}(r) = \frac{\langle \Delta s^i_{\parallel,\perp}(t,\tau) \Delta s^j_{\parallel,\perp}(t,\tau) \delta(r - R^{i,j}(t)) \rangle_{i \neq j}}{2\tau}. \quad (2)$$

Figure 2 shows the cross-correlated diffusion coefficients $D_{\parallel,\perp}(r)$ scaled by the self-diffusion coefficient $D_s(n)$ as functions of the distance r, which is scaled by the particle diameter $2a$, for sample S1. The area fraction for sample S1 ranges from 0.007 to 0.20. From Fig. 2, it can be seen that the scaled cross-correlated diffusion coefficients $D_{\parallel,\perp}(r/2a)/D_s(n)$ are invariant with the concentration n. However, the cross-correlated diffusion should be strongly influenced by the viscosity of the colloidal monolayer, which directly depends on the concentration n. The effects of the concentration n on the cross-correlated diffusion are hidden in the plots of $D_{\parallel,\perp}(r/2a)/D_s(n)$ for this sample. This finding suggests that the single-diffusion coefficient $D_s(n)$ and the particle diameter $2a$ are not good parameters with which to analyze the cross-correlated diffusion. The scaled cross-correlated diffusion coefficients $D_{\parallel,\perp}(r/2a)/D_S(n)$ for the other two samples, S2 and S3, are shown in Fig. A1 and Fig. A2 in the Appendix A. The raw data of S1 and S3 were published in Ref. [31], while data of S2 are published first time.

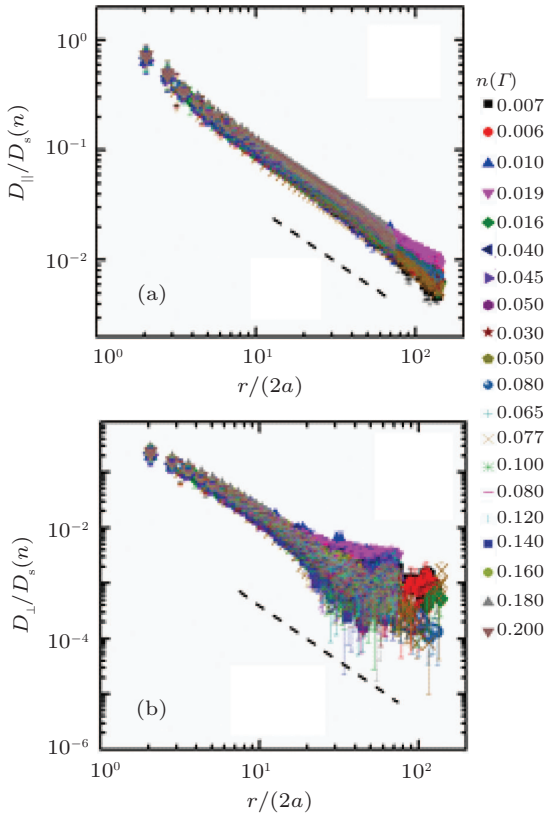


Fig. 2. Measured correlated diffusion coefficients $D_{\parallel}/D_s(n)$ (a) and $D_{\perp}/D_s(n)$ (b) as functions of $r/(2a)$ for sample S1 at different particle area fractions n on a log–log plot. The concentration n ranges from 0.007 to 0.20, and the friction coefficient of the particle monolayer ranges from 0.06 cP · μm to 3.53 cP · μm. The differently colored symbols represent different values of n and different viscosity coefficients, where the black squares correspond to $n \approx 0.007$ and the maroon inverted triangles correspond to $n \approx 0.020$. The dashed lines are guides for the eye, corresponding to $\sim 1/r$ in panel (a) and to $\sim 1/r^2$ in panel (b).

The self-diffusion coefficient for a single particle is written as $D_s(n) = k_B T/\kappa\eta a$, where κ is a dimensionless constant. $\kappa\eta a$ represents the friction experienced by one particle. For a particle in a colloidal monolayer, normally such a friction include two terms, $\Gamma^{(0)}$ and $\Gamma^{(1)}$, one related to the contribution from the surrounding liquid and the other to the contribution from the colloidal monolayer. According to Refs. [31] and [32], the self-diffusion coefficient $D_s(n)$ can be divided into two effective coefficients: $D_s(0) = k_B T/\Gamma^{(0)}$ and $D'_s(0) = k_B T/\Gamma^{(1)}$, where $\Gamma^{(0)} = \kappa^{(0)}\eta_b a$ and $\Gamma^{(1)} = \kappa^{(1)}\eta_s$. Parameters $\kappa^{(0)}$ and $\kappa^{(1)}$ are two dimensionless coefficients. The term $\Gamma^{(0)}$ is the friction coefficient of the colloidal monolayer in the dilute limit ($n = 0$), which reflects the influence of the local environment of the liquid. The other term, $\Gamma^{(1)}$, is the friction coefficient of the colloidal monolayer at concentrations of $n > 0$, which is influenced by the many-body effect of the particles. The effective diffusion $D_s(0)$ can be obtained by means of a fit parameter α as follows: $D_s(0) = \alpha \cdot D_0$. $D'_s(n)$ can be calculated from the equation $1/D_s(n) = 1/D_s(0) + 1/D'_s(n)$.[31,32] The effective diffusion $D'_s(n)$ depends on the concentration n. As shown in Fig. 3, $D'_s(n)$ exhibits an inverse relation with n, as expressed by $D'_s/D_s(n) = 1 + 3/2n$, for each of the three samples. As shown in the inset of Fig. 3, such a relationship is a general description for all samples when $n < 0.1$. The value 3/2 in the above equation could be estimated by the inverse value of averaged β in Table 1.

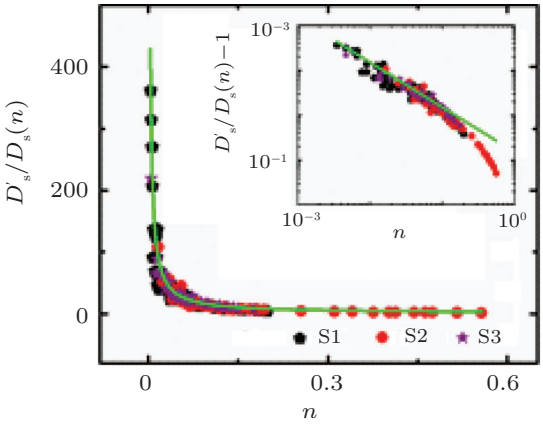


Fig. 3. The calculated $D'_s(n)$ values scaled by $D_s(n)$ as a function of the area fraction n for all three samples: S1 (black pentagon), S2 (red dot), and S3 (purple star). The green line shows the fit to $D'_s(n)/D_s(n) = 1 + 3/(2n)$. A log–log replot of $D'_s(n)/D_s(n) - 1$ *versus* n is shown in the inset, where a green line with a slope of -1 is plotted as eye guide.

Because $\Gamma^{(0)}$ represents the friction experienced by a single particle in dilute limit and only $\Gamma^{(1)}$ represents the friction contributed by the interaction between the particles in the monolayer.[29] Considering that $D_{\parallel,\perp}$ reflects the strength of HIs between the particles, the change of $D_{\parallel,\perp}$ induced by n is contributed only by the change of $\Gamma^{(1)}$, and has nothing to do with $\Gamma^{(0)}$. After all, $\Gamma^{(1)}$ is a function of n, while $\Gamma^{(0)}$ is a constant and independent of n. Thus, the effective diffusion coefficient $D'_s(n)$, which only relates to the friction coefficient $\Gamma^{(1)}$, is a more suitable scaling factor than $D_s(n)$.

The plots of $D_{\parallel,\perp}/D_s$ in Fig. 2 should thus be replaced with plots of $\widetilde{D}_{\parallel,\perp} = D_{\parallel,\perp}/D'_s$. In Figs. A3–A5 in Appendix A, the plots of $\widetilde{D}_{\parallel,\perp}(r/2a)$ increase with increasing $\Gamma^{(1)}$, showing an influence of the concentration n, as expected. Moreover, new characteristic lengths should be determined to normalize the distance r to obtain a universal function of cross-correlated diffusion.

As shown in Figs. 4(a) and 4(b), all of the scaled cross-correlated diffusion coefficients $\widetilde{D}_{\parallel,\perp}$ collapse to single master curves when the distance r is scaled by an adjustable parameter $R_{\parallel,\perp}$ to obtain $r'_{\parallel,\perp} = r/R_{\parallel,\perp}$. The scaled cross-correlated diffusion coefficients $\widetilde{D}_{\parallel,\perp}(r'_{\parallel,\perp})$ for large values of $\Gamma^{(1)}$ fall on the upper left sides of the corresponding master curves, and for small values of $\Gamma^{(1)}$, they fall on the lower right sides. The curves indicate that the scaled correlation coefficients $\widetilde{D}_{\parallel,\perp}(r'_{\parallel,\perp})$, representing the strength of the HIs, are strong for a colloidal monolayer with a high $\Gamma^{(1)}$. For the other two samples, we obtained similar results using the same method (see Figs. 4(c)–4(f)). The scaled cross-correlated diffusion coefficients for all three samples with different separations collapse to single master curves, as shown in Figs. 4(g) and 4(h). The universal master curves for the different samples indicate that the HIs in a particle monolayer near a water-oil interface can be described by the same rule, even for monolayers containing particles of different sizes or lying at different separation distances from the interface. It is noted that a bit of curvature of plots in Fig. 4(h) occurs when r approaches the particle size, since a logarithmic dependence of $D(r)$ will be introduced in the short limit of r.

The universal master curves can be obtained only with suitable parameters $R_{\parallel,\perp}$. As length scales, $R_{\parallel,\perp}$ can be regarded as characteristic lengths of the system. The question then becomes how these characteristic lengths should be interpreted. In the Saffman model,[27] the characteristic length of a membrane is $\lambda_s = \eta_s/\eta_b$, which depends on the viscosity of the membrane. Based on the concept of λ_s, we define an effective Saffman length λ_s^* for a particle monolayer near a water–oil interface, expressed as $\lambda_s^* = \Gamma^{(1)}/6\pi\eta_b$. The effective Saffman length is the ratio of the friction coefficient $\Gamma^{(1)}$ of the particles in the monolayer to the traditional friction coefficient $6\pi\eta_b$ of the particles in a bulk liquid. In the present system, the effective coefficient λ_s^* is written as $\lambda_s^* = \Gamma^{(1)}/(6\pi \cdot (\eta_w + \eta_o)/2$. The characteristic length $R_{\parallel}$ in

the longitudinal direction is taken to be equal to λ_s^*, as shown in Eq. (3):

$$R_{\parallel} = \lambda_s^*. \tag{3}$$

From Eq. (3) and the definition of λ_s^*, the friction coefficient values $\Gamma_{\parallel}^{(2)}$ can be obtained from $R_{\parallel} = \Gamma_{\parallel}^{(2)}/(6\pi\cdot(\eta_w + \eta_o)/2)$. The superscript and subscript of $\Gamma_{\parallel}^{(2)}$ suggest that this friction coefficient can be estimated from two-particle diffusion measurements in the longitudinal direction. Meanwhile, $\Gamma^{(1)}$ can also be obtained from single-particle diffusion measurements, in accordance with the formulas $D_s'(n) = k_B T/\Gamma^{(1)}$ and $1/D_s(n) = 1/D_s(0) + 1/D_s'(n)$.

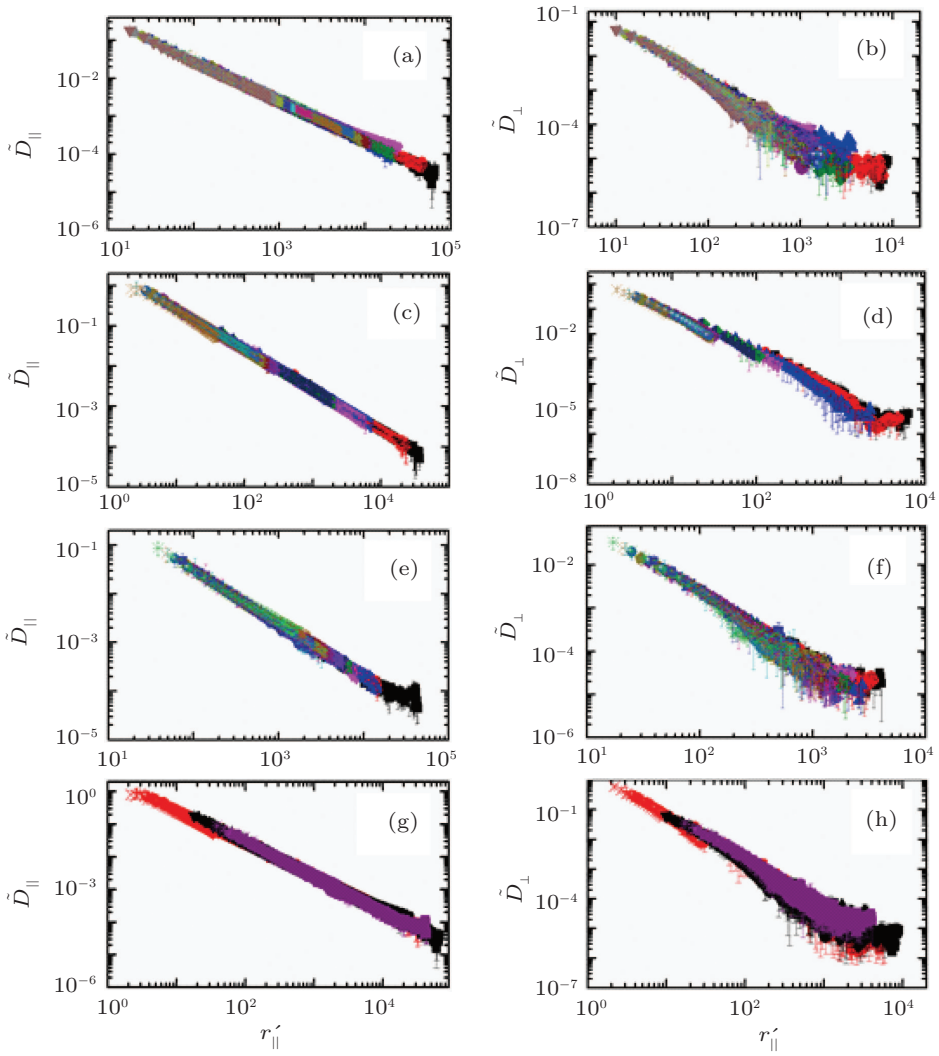


Fig. 4. Scaled correlated diffusion coefficient $\widetilde{D}_{\parallel}$ as a function of the scaled distance $r'_{\parallel}$ for samples S1 (a), S2 (c), S3 (e). Scaled correlated diffusion coefficient $\widetilde{D}_{\perp}$ as a function of the scaled distance $r'_{\perp}$ for samples S1 (b), S2 (d), S3 (f). The differently colored symbols represent different values of n. The concentration n ranges from 0.007 to 0.2 for S1 [panels (a) and (b)], from 0.02 to 0.62 for S2 [panels (c) and (d)], from 0.005 to 0.18 for S3 [panels (e) and (f)]. The comparison of three master curves $\widetilde{D}_{\parallel}(r'_{\parallel})$ (g) and $\widetilde{D}_{\perp}(r'_{\perp})$ (h) for all samples: S1 (black), S2 (red), and S3 (purple). The symbols used in panels (a) and (b) are the same as those in Fig. 2. The symbols used in panels (c) and (d) are the same as those in Fig. A1 in the appendix. The symbols used in panels (e) and (f) are the same as those in Fig. A2 in the appendix.

As shown in Fig. 5(a), the $\Gamma_{\parallel}^{(2)}$ values obtained from $R_{\parallel}$ agree with the $\Gamma^{(1)}$ values obtained from $D_s'(n)$, which justifies the rationality of the relationship $R_{\parallel} = \lambda_s^*$. However, in the transverse direction, the equivalent of Eq. (3), $R_{\perp} = \lambda_s^*$, does not work as the characteristic length. If $R_{\perp} = \lambda_s^*$ is assumed, then the friction coefficient $\Gamma_{\perp}^{(2)}$ obtained from $\lambda_s^* = \Gamma_{\perp}^{(2)}/(6\pi\cdot(\eta_w + \eta_o)/2)$ is not a linear function of $\Gamma^{(1)}$. In fact, $\Gamma_{\perp}^{(2)}$ will exhibit a power-law relationship with $\Gamma^{(1)}$, expressed as $\Gamma_{\perp}^{(2)} \sim (\Gamma^{(1)})^{2/3}$. Such a wrong dependence of $\Gamma_{\perp}^{(2)}$ on $\Gamma^{(1)}$ given by the assumption ($R_{\perp} = \lambda_s^*$) is shown in Fig. 5(b), as a comparison of the correct dependence in Fig. 5(a). As suggested by this power-law relationship, the transverse characteristic length $R_{\perp}$ should instead be written as

$$R_{\perp} = a\left(\frac{\lambda_s^*}{a}\right)^{2/3}, \tag{4}$$

for $\Gamma_{\perp}^{(2)} = \Gamma^{(1)}$ to be satisfied, where $\lambda_s^* = \Gamma_{\perp}^{(2)}/(6\pi \cdot (\eta_w + \eta_o)/2)$.

The plot of $\Gamma_{\perp}^{(2)}$ *versus* $\Gamma^{(1)}$ is shown in Fig. 5(a). Both $\Gamma_{\parallel}^{(2)}$ and $\Gamma_{\perp}^{(2)}$ are friction coefficients obtained for the same colloidal monolayer. Unsurprisingly, $\Gamma_{\parallel}^{(2)}$ and $\Gamma_{\perp}^{(2)}$ should be equal to each other, as shown in the inset of Fig. 5(a). Thus, we can define the friction coefficient obtained from cross-correlated diffusion as $\Gamma^{(2)}$, where $\Gamma^{(2)} = \Gamma_{\parallel}^{(2)} = \Gamma_{\perp}^{(2)}$. The characteristic lengths $\Gamma_{\parallel}$ and $\Gamma_{\perp}$ follow Eq. (3) and Eq. (4), respectively, indicating that the HIs are anisotropic in the two orthogonal directions. By combining Eq. (3) and Eq. (4), the relationship between $R_{\parallel}$ and $R_{\perp}$ can be found to be $R_{\parallel}/a = (R_{\perp}/a)^{3/2}$, as shown in Fig. 5(c).

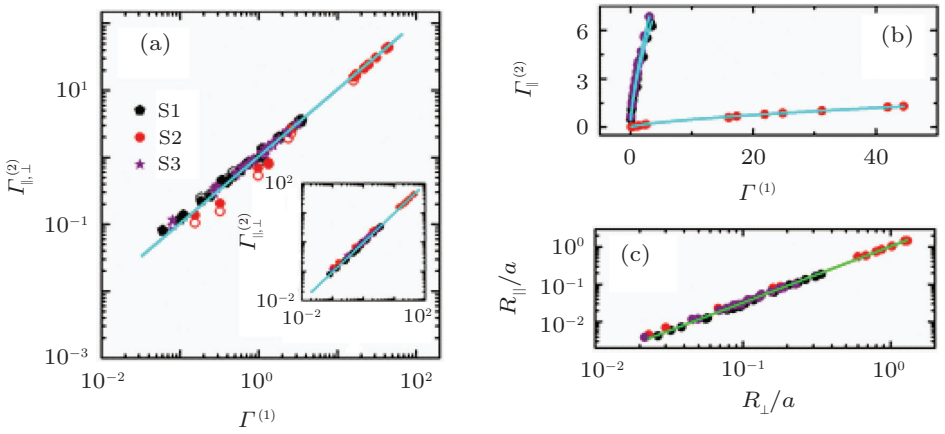


Fig. 5. (a) Comparison between the friction coefficients $\Gamma^{(1)}$ calculated from $D_s'(n)$ and the friction coefficients $\Gamma_{\parallel,\perp}^{(2)}$ of the three samples S1 (black pentagon), S2 (red dot), and S3 (purple star) on a log–log plot. The solid dots correspond to $\Gamma_{\parallel}^{(2)}$, and the open dots correspond to $\Gamma_{\perp}^{(2)}$. The cyan line is the guide for the eye, where the slope of the line is 1.0. In the inset, a comparison is shown between the friction coefficients $\Gamma_{\parallel}^{(2)}$ and $\Gamma_{\perp}^{(2)}$ on a log–log plot. The cyan line is the guide for the eye, where the slope of the line is 1.0. (b) The friction coefficient $\Gamma_{\perp}^{(2)}$ obtained from $R_{\perp} = \lambda_s$ follows a power-law relationship with the friction coefficient $\Gamma^{(1)}$ for the three samples. The cyan lines represent fits of the form $\Gamma_{\perp}^{(2)} \sim (\Gamma^{(1)})^{2/3}$. (c) Relationship between the characteristic lengths $R_{\parallel}$ and $R_{\perp}$ scaled by the particle radius a for the three samples on a log–log plot. The green line is the fit to $R_{\parallel}/a = (R_{\perp}/a)^{3/2}$.

By the definition of cross-correlated diffusion coefficients, the values of $D_{\parallel,\perp}$ can be written as $D_{\parallel,\perp} \propto D_s(0) \cdot f(\Gamma^{(1)}, r)$. Here, the dimensionless factor of $f(\Gamma^{(1)}, r)$ represents the strength of the correlation between two particles in the monolayer. Moreover, $D_s'(n)$ can be also written as $D_s'(n) \propto D_s(0) \cdot g(\Gamma^{(1)}(n))$, since both $D_s'(n) = k_B T/\kappa^{(1)}\eta_s$ and $D_s(0) = k_B T/\kappa^{(0)}\eta_b a$ are proportional to $k_B T$ and η_s is a function of $\eta_b a$. Therefore, the effective diffusion constants $D_s'(n) = k_B T/\Gamma^{(1)}$ should be used as the scaling factor for different monolayers. The scaled curves by using $D_s(n)$, as shown in Fig. 2 and A2, either just simply overlap without a right order, or apparently diverse (Fig. A1). Only when $D_s'(n)$ are used as scaling factor, can the scaled curves be ranked into a general master curve with a correct order (Fig. 4) for all independent samples (S1, S2 and S3): the curves for large values of $\Gamma^{(1)}$ fall on the upper left side, the curves for small values of $\Gamma^{(1)}$ fall on the bottom right side.

In Figs. 2(a) and 2(b), $D_{\parallel}/D_s(n)$ for sample S1 decays with the distance r as $\sim 1/r$ in the limit of large r, while $D_{\perp}/D_s(n)$ decays as $\sim 1/r^2$. These behaviors are the result of the anisotropic HIs in a colloidal monolayer near a liquid–liquid interface. In the longitudinal direction, the HIs respond to a 3D shear stress that is similar to that in a 3D bulk liquid, and in the transverse direction, the HIs respond to a 2D compressive stress.[13,26] The propagation of the vertical component of momentum through the interface will be diminished due to the surface tension of the water–oil interface, otherwise the curved interface will cost extra energy. Meanwhile, the horizontal component of the momentum can propagate freely in the system, which results in the quasi-2D HIs of $D_{\parallel} \sim 1/r$ and $D_{\perp} \sim 1/r^2$ between the particles in the monolayer near a water–oil interface, rather than the HIs of $D_{\parallel,\perp} \sim 1/r$ in the 3D bulk liquid. The anisotropy of the characteristic lengths $R_{\parallel}$ and $R_{\perp}$ of a colloidal monolayer near a water–oil interface is also similar to that near a water–air interface.[32] This anisotropic behavior can be explained by analogy to the lubrication force between two solid walls.[32,37]

It is worth noting that the particles also fluctuate in the direction perpendicular to the water–oil interface due to the temperature. The amplitude of fluctuation Δz can be estimated through $k_B T/2 = \Delta m \cdot g \cdot \Delta z$, with $\Delta m = m_{\text{particle}} - m_{\text{water}}$. The value of $\Delta z/z$ for three samples S1, S2, and S3 are 0.27, 0.03, and 0.41, respectively. In principle, the vertical fluctuation of particles Δz will be modified by the HIs between the particles among the monolayer. As shown in Figs. 4(e) and 4(h), the master curves with different Δz and z are collapsed together directly, which suggests that the effect of vertical fluctuation of particles on HIs between particles are also included in $D_s'(n) = k_B T/\kappa^{(1)}\eta_s$, since the values of $\kappa^{(1)}$ and η_s already involves the effect of z and Δz.

In the system of a water–oil interface, the scaled correlated diffusion coefficients $\widetilde{D}_{\parallel,\perp}(r'_{\parallel,\perp})$ are independent on the separation z, as seen in Figs. 4(g) and 4(h), while $\widetilde{D}_{\parallel,\perp}(r'_{\parallel,\perp})$

in the water–air system are dependent on the separation z.[32] Comparing these two systems, the significant difference is that the viscosity and mass density of the air can be negligible comparing with oil. HIs contributed by the oil overwhelms small change of HIs resulting from the different locations of colloidal monolayers. In the colloidal monolayer near the water–air interface, the momentum (stress flux) of the monolayer diffuse only into one side of the interface, *i.e.*, the region of water. The HIs near the water–air interface is sensitive to the thickness of the water film between the monolayer and the interface. In the water–oil system, the momentum (stress flux) of the monolayer diffuse into both sides of the interface, *i.e.*, the regions of water and oil. Comparing with the influence of the bulk of water and oil, the influence of the thin water film between the monolayer and the water–oil interface can be negligible. The diffusion of the momentum (stress flux) into the whole space causes that $\widetilde{D}_{\parallel,\perp}(r'_{\parallel,\perp})$ in the water–oil system is insensitive to the separation (as shown in Fig. 4).

The high viscosity of oil may also cause the curves collapse Fig. 2 (Sample S1) and Fig. A2 (Sample S3), since such collapse was never found in monolayers near a water–air interface.[32] We think the difference of $D_{\parallel,\perp}$ induced by the change of particle concentrations lie already in $D_s(n)$, but only in the part of $D'_s(n)$. $D_s(0)$ is just a constant and independence on n. It is the reason why the rescaling method in Fig. 4 works so well for all the situations.

3. Conclusion

In this work, we measured the cross-correlated diffusion in particle monolayers near a water–oil interface. An effective Saffman length of $\lambda_s^* = \kappa^{(1)}\eta_s/6\pi\eta_b$ was defined for such a colloidal monolayer On the basis of this effective Saffman length, anisotropic characteristic lengths $R_\parallel$ and $R_\perp$ were introduced in the longitudinal and transverse directions, respectively. In the longitudinal direction, the characteristic length $R_\parallel$ is equal to λ_s^*, which reflects the continuous nature of the system. In the transverse direction, the characteristic length $R_\perp$ is a function of λ_s^* and the particle radius a, with the form $a(\lambda_s^*/a)^{2/3}$, which reflects the discrete nature of the system. The anisotropy of the characteristic lengths reflects the fundamental differences in the dynamics of the colloidal monolayer in the two directions. With these two characteristic lengths, the measured curves of the cross-correlated diffusion for three samples at different concentrations collapse to universal master curves. These universal master curves describe the HIs in a particle monolayer near a soft interface. This experimental research provides a general picture of the dynamics of a liquid near an interface.

Appendix A: Supplementary figures

The scaled cross-correlated diffusion coefficients for three samples are shown in the following figures.

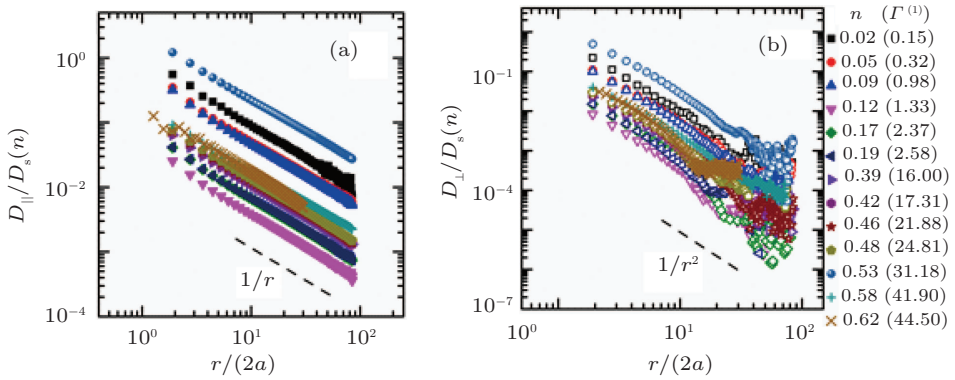


Fig. A1. Measured correlated diffusion coefficients $D_\parallel/D_s(n)$ (a) and $D_\perp/D_s(n)$ (b) as functions of the distance $r/(2a)$ for sample S2. The concentration ranges from 0.02 to 0.62, and the friction coefficient of the particle monolayer ranges from 0.15 cP · μm to 44.5 cP · μm. The differently colored symbols represent the scaled correlated diffusion coefficients at different friction coefficients.

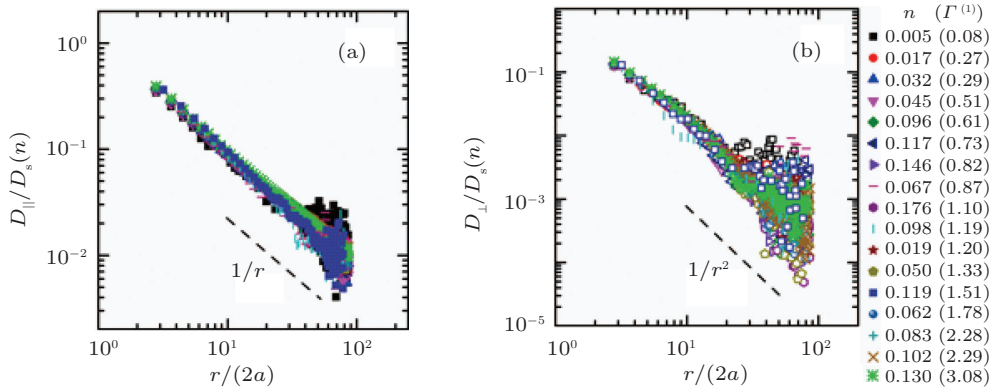


Fig. A2. Measured correlated diffusion coefficients $D_\parallel/D_s(n)$ (a) and $D_\perp/D_s(n)$ (b) as functions of the distance $r/(2a)$ for sample S3. The concentration n ranges from 0.005 to 0.18, and the friction coefficient of the particle monolayer ranges from 0.08 cP · μm to 3.08 cP · μm. The differently colored symbols represent the scaled correlated diffusion coefficients at different friction coefficients.

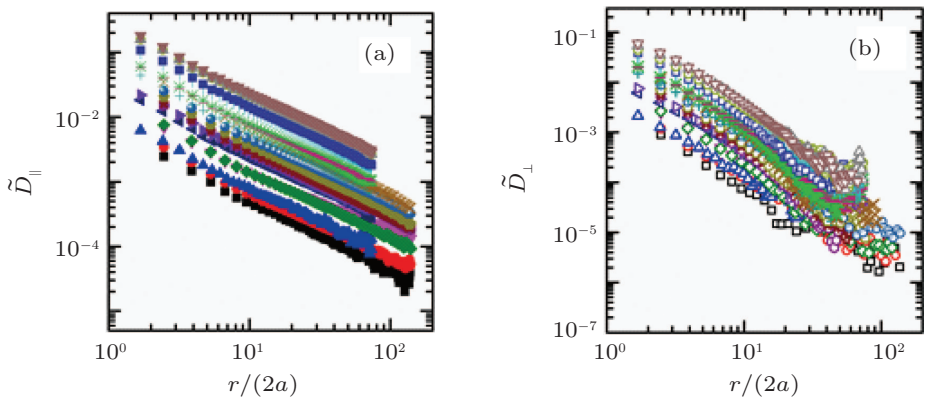


Fig. A3. Scaled correlated diffusion coefficients $\widetilde{D}_{\parallel}$ (a) and $\widetilde{D}_{\perp}$ (b) as functions of $r/(2a)$ with different friction coefficients for sample S1. The differently colored symbols represent the scaled correlated diffusion coefficients at different friction coefficients. The symbols used in this figure are the same as those in Fig. 2.

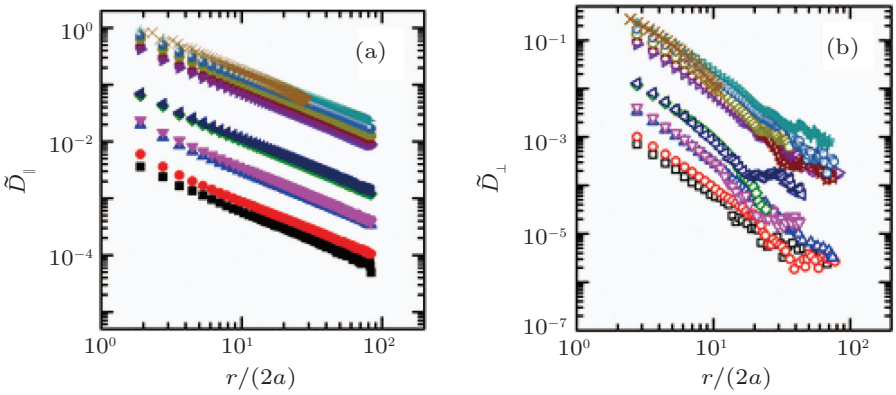


Fig. A4. Scaled correlated diffusion coefficients $\widetilde{D}_{\parallel}$ (a) and $\widetilde{D}_{\perp}$ (b) as functions of $r/(2a)$ with different friction coefficients for sample S2. The differently colored symbols represent the scaled correlated diffusion coefficients at different friction coefficients. The symbols used in this figure are the same as those in Fig. A1.

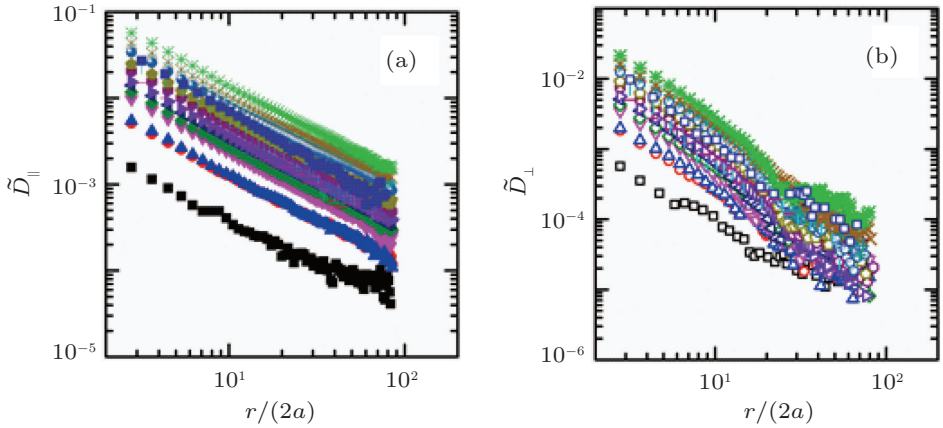


Fig. A5. Scaled correlated diffusion coefficients $\widetilde{D}_{\parallel}$ (a) and $\widetilde{D}_{\perp}$ (b) as functions of $r/(2a)$ with different friction coefficients for sample S3. The differently colored symbols represent the scaled correlated diffusion coefficients at different friction coefficients. The symbols used in this figure are the same as those in Fig. A2.

References

[1] Wang C J, Ackerman D M, Slowing I I and Evans J W 2014 *Phys. Rev. Lett.* **113** 038301

[2] Rienzo C D, Piazza V, Gratton E, Beltram F and Cardarelli F 2014 *Nat. Commun.* **5** 5891

[3] Levine A J and Lubensky T C 2000 *Phys. Rev. Lett.* **85** 1774

[4] Frydel D and Diamant H 2010 *Phys. Rev. Lett.* **104** 248302

[5] Shani I, Beatus T, Bar-Ziv R H and Tlusty T 2014 *Nat. Phys.* **10** 140

[6] Lutz C, Kollmann M and Bechinger C 2004 *Phys. Rev. Lett.* **93** 026001

[7] Misiunas K, Pagliara S, Lauga E, Lister J R and Keyser U F 2015 *Phys. Rev. Lett.* **115** 038301

[8] Beatus T, Tlusty T and Bar-Ziv R 2006 *Nat. Phys.* **2** 743

[9] Cui B, Diamant H and Lin B 2002 *Phys. Rev. Lett.* **89** 188302

[10] Wang C Y, Zhang C B, Huang X Y, Liu X D and Chen Y P 2016 *Chin. Phys. B* **25** 108202

[11] Li H H, Zheng Z Y and Wang Y R 2019 *Chin. Phys. Lett.* **36** 034701

[12] He W, Song H, Su Y, Geng L, Ackerson B J, Peng H B and Tong P 2016 *Nat. Commun.* **7** 11701

[13] Oppenheimer N and Diamant H 2009 *Biophys J.* **96** 3041

[14] Gambin Y, Lopez-Esparza R, Reffay M, Sierecki E, Gov N S, Genest M, Hodges R S and Urbach W 2006 *Proc. Natl. Acad. Sci. USA* **103** 2098
[15] Huang K and Szlufarska I 2015 *Nat. Commun.* **6** 8558
[16] Cui B, Diamant H, Lin B and Rice S A 2004 *Phys. Rev. Lett.* **92** 258301
[17] Cichocki B, Ekiel-Jezewska M L and Wajnryb E 2007 *J. Chem. Phys.* **126** 184704
[18] Brotto T, Caussin J B, Lauga E and Bartolo D 2013 *Phys. Rev. Lett.* **110** 038101
[19] Wang G M, Prabhakar R and Sevick E M 2009 *Phys. Rev. Lett.* **103** 248303
[20] Kaveh F, Ally J, Kappl M and Butt H J 2014 *Langmuir* **30** 11619
[21] Ishak N I, Muniandy S V, Periasamy V, Ng F L and Phang S M 2017 *Chin. Phys. B* **26** 088203
[22] Prasad V, Koehler S A and Weeks E R 2006 *Phys. Rev. Lett.* **97** 176001
[23] He D H, Yang T, Li W H, Zhang Q L and Ma H R 2007 *Chin. Phys. B* **16** 3138
[24] Prasad V and Weeks E R 2009 *Phys. Rev. Lett.* **102** 178302
[25] Nguyen Z H, Atkinson M, Park C S, Maclennan J, Glaser M and Clark N 2010 *Phys. Rev. Lett.* **105** 268304
[26] Oppenheimer N and Diamant H 2010 *Phys. Rev. E* **82** 041912
[27] Saffman P G and Delbruck M 1975 *Proc. Natl. Acad. Sci. USA* **72** 3111
[28] Vivek S and Weeks E R 2015 *PLoS ONE* **10** e0121981
[29] Cheung C, Hwang Y H, Wu X and Choi H J 1996 *Phys. Rev. Lett.* **76** 2531
[30] Saffman P G 1976 *J. Fluid Mech.* **73** 593
[31] Zhang W, Li N, Bohinc K, Tong P and Chen W 2013 *Phys. Rev. Lett.* **111** 168304
[32] Li N, Zhang W, Jiang Z and Chen W 2018 Preprint at http://arxivorg/abs/180810649
[33] Zhang W, Chen S, Li N, Zhang J Z and Chen W 2014 *PLoS ONE* **9** e85173
[34] Crocker J C and Grier D G 1996 *J. Colloid Interface Sci.* **179** 298
[35] Chen W and Tong P 2008 *Europhys Lett.* **84** 28003
[36] Wang G M, Prabhakar R, Xgao Y and Sevick E M 2011 *J. Opt.* **13** 044009
[37] Hamrock B J, Schmid S R and Jacobson B O 2004 *Fundamentals of Fluid Film Lubrication*, 2nd edn. (New York: Marcei Dekker, Inc.)